



T.C.
YÜKSEKÖĞRETİM KURULU BAŞKANLIĞI
ANKARA

05.03.2024

OKUL TANIMA BELGESİ

T.C. Kimlik No : 44749306658
Adı Soyadı : İSMAIL ALTUNTAŞ
Ülke : RUSYA FEDERASYONU
Üniversite : National Research Nuclear University "MEPHI"
Durumu : Kurulumuzda mevcut uluslararası listelerde yer almaktadır.

Açıklama

Yurtdışındaki yükseköğretim kurumlarından örgün eğitim yoluyla alınan diplomaların denklik işlemi, 2547 sayılı Yükseköğretim Kanunu'nun 2880 sayılı kanunla değişik 7/p maddesi ile 05.12.2017 tarihli Resmi Gazete'de yayımlanan "Yurtdışı Yükseköğretim Diplomaları Tanıma ve Denklik Yönetmeliği" hükümleri uyarınca yapılmakta olup, söz konusu Yönetmelik yatay geçiş, dikey geçiş ve lisans tamamlama gibi kavramları kapsamamaktadır.

Yurtdışındaki yükseköğretim kurumlarından uzaktan öğretim yoluyla alınacak diplomalar ise söz konusu Yönetmeliğin 10. maddesi ve ilgili mevzuat çerçevesinde değerlendirilmektedir.

Öğrenim dili Türkçe olan yurt dışındaki yükseköğretim programlarından alınan diplomalar için yapılan başvurular Yönetmelik'in 7. madde, 6. fıkra, (ç) bendi "*Türkiye'nin taraf olduğu uluslararası anlaşmalarla öğrenim dilinin Türkçe olduğu belirlenen programlar veya Yükseköğretim Kurulunca tanınan yurtdışındaki Türkçe yükseköğretim programları dışında, yükseköğretim kurumlarının açtığı ve öğrenim dili Türkçe olan programlardan alınan diplomalar için yapılan başvurular reddedilir.*" hükmü çerçevesinde karara bağlanacaktır.

Diploma denklik başvurusunda aranacak belgeler ile inceleme ve değerlendirme usul ve esasları Yurtdışı Yükseköğretim Diplomaları Tanıma ve Denklik Yönetmeliği'nde belirtilmiş olup; ilgili Yönetmelik ve detaylı bilgiye Yükseköğretim Kurulu web sayfasından ulaşılabilmektedir.

Yatay geçiş başvuruları, 08.02.2008 tarih ve 636/2732 sayılı yazımız ile "Yükseköğretim Kurumları Arasında Ön lisans ve Lisans Düzeyindeki Programlar Arasında Geçiş, Çift Anadal, Yan Dal ile Kurumlar Arası Kredi Transferi Yapılması Esaslarına İlişkin Yönetmelik" hükümlerine; lisansüstü eğitim başvuruları ise 26.09.2017 tarih ve 64528 sayılı yazı ile "Lisansüstü Eğitim ve Öğretim Yönetmeliği" hükümlerine uygun olarak, alınan dersler incelenmek suretiyle başvuru yapılan Üniversite tarafından değerlendirilmekte ve karara bağlanmaktadır.

2547 Sayılı Kanun'un 11 b/5 maddesi uyarınca yurtdışında yapılan doktora eğitimleri Üniversitelerarası Kurul tarafından değerlendirilmektedir. Yurtdışında yapılan doktora eğitiminin Türkiye'de yapılan doktora eşdeğer olup olmayacağı hususunda önceden herhangi bir görüş belirtmek mümkün olmadığı gibi, söz konusu eşdeğerlik, doktora tamamlandıktan sonra ilgili komisyon ve kurullar tarafından incelenmektedir.

Öte yandan diploma denklik başvuruları, ilgili Komisyon ve Kurullar tarafından münferiden değerlendirildiğinden yurt dışındaki yükseköğretim kurumlarından alınmış ön lisans, lisans ve yüksek lisans diplomalarının ülkemizdeki diplomalara eşdeğer olup olmayacağı hususunda önceden herhangi bir görüş belirtmek mümkün olmadığı gibi, eğitim alınan yükseköğretim kurumunun tanınırlığına ilişkin olarak Kurulumuzun yeni kararlar alma hakkı saklıdır.

Yurt dışında yükseköğrenim görmek isteyen öğrencilerin konuyla ilgili güncel gelişme ve kararları Kurulumuz internet adresinden takip etmeleri yararlarına olacaktır.

Bilgilerinizi rica ederim.

***BU BELGE DENKLİK BELGESİ YERİNE GEÇMEZ**

Bu belgenin doğruluğunu barkod numarası ile <https://www.turkiye.gov.tr/belge-dogrulama> adresinden, mobil cihazlarınıza yükleyeceğiniz e-Devlet Kapısına ait Barkodlu Belge Doğrulama veya YÖK Mobil uygulaması vasıtası ile yandaki karekod okutularak kontrol edilebilir.



Search > Results for Physica B-Condensed Matter (All Fields)

24,476 results from Web of Science Core Collection for:

Analyze Results

Physica B-Condensed Matter (All Fields)

+ Add Keywords

Quick add keywords: <

+ NON-FERMI LIQUID

+ MUONIUM

+ POLARIZED NEUTRONS

+ MU SR

+ HEAVY FERMIONS

+

Publications

You may also like...

Refine results

Search within results...

Quick Filters

- Review Article 76
- Open Access 1,973
- Enriched Cited References 973

Publication Years ⓘ

- 2024 19
- 2023 680
- 2022 786
- 2021 732
- 2020 538

See all >

Document Types

- Article 24,181
- Proceeding Paper 10,541

0/24,476

Add To Marked List

Export ▾

Sort by: f

1 Frank de Boer retires from the board of editors of Physica B: Condensed Matter

Buschow, KHJ

Dec 1 2019 | PHYSICA B-CONDENSED MATTER 574

Full Text at Publisher ...

2 Comment on the paper "Comparative investigation of five nanoparticles in flow of viscous fluid with J and slip due to rotating disk, Sumaira Qayyum, Muhammad Ijaz Khan, Tasawar Hayat, Ahmed Alsaedi, Condensed Matter 534 (2018) 173-183"

Pantokratoras, A

Jun 15 2021 | Apr 2021 (Early Access) | PHYSICA B-CONDENSED MATTER 611

Full Text at Publisher ...

3 Estimation of distance-distribution probabilities from pulsed electron paramagnetic resonance (EPR) data of two

← Journal information

×

PHYSICA B-CONDENSED MATTER

Publisher name: ELSEVIER

Journal Impact Factor™

2.8

2022

2.3

Five Year

JCR Category	Category Rank	Category Quartile
PHYSICS, CONDENSED MATTER <i>in SCIE edition</i>	34/67	Q3

Source: Journal Citation Reports 2022. Learn more

Journal Citation Indicator™ New

0.52

2022

0.47

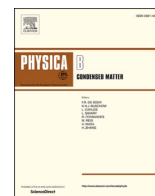
2021

JCI Category	Category Rank	Category Quartile
PHYSICS, CONDENSED MATTER <i>in SCIE edition</i>	36/76	Q2

The Journal Citation Indicator is a measure of the average Category Normalized Citation Impact (CNCI) of citable items (articles and reviews) published by a journal over a recent three year period. It is used to help you evaluate journals based on other metrics besides the Journal Impact Factor (JIF).

Learn more

Related records



Investigating the optical, electronic, magnetic properties and DFT of NiO films prepared using RF sputtering with various argon pressures

Hicret Hopoğlu^{a,b}, Dogan Kaya^{c,d,*}, Mikhail M. Maslov^e, Savas Kaya^f, İlkyay Demir^{b,g}, İsmail Altuntaş^{b,g}, Fatih Urgan^a, Mustafa Akyol^h, Ahmet Ekicibil^c, Ebru Şenadım Tüzemen^{a,b,**}

^a Department of Physics, Sivas Cumhuriyet University, 58140, Sivas, Turkey

^b Nanophotonics Research and Application Center, Sivas Cumhuriyet University, 58140, Sivas, Turkey

^c Department of Physics, Faculty of Art and Sciences, Cukurova University, 01330, Adana, Turkey

^d Department of Advance Materials and Nanotechnology, Graduate School of Sciences, Cukurova University, Adana, 01330, Turkey

^e Department of Condensed Matter Physics, National Research Nuclear University "MEPhI", Kashirskoe Shosse 31, 115409, Moscow, Russia

^f Health Services Vocational School, Department of Pharmacy, Sivas Cumhuriyet University, 58140, Sivas, Turkey

^g Department of Nanotechnology Engineering, Sivas Cumhuriyet University, 58140, Sivas, Turkey

^h Department of Materials Science and Engineering, Faculty of Engineering, Adana Alparslan Turkes Science and Technology University, 01250, Adana, Turkey

ARTICLE INFO

Keywords:

NiO
Sputtering
Optical
Electronic
Magnetization
DFT

ABSTRACT

In this study, we investigated the structural, optical, magnetic, and conductive properties of nickel oxide (NiO) films on glass substrates deposited using Radio Frequency (RF) magnetron sputtering with varying Ar gas pressure and thickness. X-ray diffraction and Rietveld refinement analysis confirmed a cubic crystal structure and showed that the lattice parameters and the $d_{(111)}$ -space increased from 4.0559 Å to 4.2712 Å and from 2.3208 Å to 2.4582 Å, respectively, due to increased Ar pressure during deposition. Scanning electron microscopy and atomic force microscopy were used to determine the cross-sectional and surface topology of the NiO films, which exhibited uniform and homogeneous growth with an average spherical size of 54.28 ± 0.33 nm. The optical bandgap values of the films were calculated to be between 3.26 and 3.65 eV, increasing with pressure. Hall measurements confirmed the p-type semiconductor nature of the films with an average sheet carrier density of 10^{10} cm⁻². The films exhibited soft magnetic properties, with a maximum H_c and M_s of 178.5 Oe and 5.82 emu/cm³ for 246 nm NiO film, respectively. Density functional theory (DFT) calculations confirmed the experimental results for both single to five layers NiO films and bulk NiO formations. The refined energy gap value was found to be 3.2 eV by the DFT calculation. The films produced at room temperature were found to be stable and reproducible, making them suitable as p-type materials for device construction.

1. Introduction

Nickel Oxide (NiO) is a highly promising transition metal oxides due to its applications in spin valve heterostructures, antiferromagnetic layers, gas sensors, optoelectronic devices, and organic light-emitting diodes [1–5]. Despite its high resistivity [6] and wide bandgap of 3.2–4.0 eV [7], NiO is an insulator at room temperature and exhibits antiferromagnetic behavior below the Néel temperature, $T_N = 523$ K [8]. Both physical and chemical methods have been used to prepare pure NiO nanoparticles or thin films, with physical methods such as

magnetron sputtering, physical vapor deposition, pulsed laser deposition, and metal oxidation being successful methods for producing high-purity and uniform films [9–13]. The magnetron sputtering technique is particularly advantageous for producing NiO films as it provides a low-cost, pure, and large-area option. Herein, the radio frequency (RF) sputter power, Ar, N, and O₂ gases/pressures, deposition time and substrates are important parameters to produce desired thin films [14–19].

The effect of deposition temperature, power, and gases such as Ar, N, O₂ during RF sputtering have been studied to control the structural

* Corresponding author. Department of Physics, Faculty of Art and Sciences, Cukurova University, 01330, Adana, Turkey.

** Corresponding author. Department of Physics, Sivas Cumhuriyet University, 58140, Sivas, Turkey.

E-mail addresses: dogankaya@cu.edu.tr (D. Kaya), esenadim@cumhuriyet.edu.tr (E.Ş. Tüzemen).

properties of various film formations to achieve desired optical, conductive, magnetic, catalytic, mechanic, properties etc. [20–24]. For example, increasing the sputtering power from 100 W to 300 W increases the crystallinity, size, and optical band gap of $\text{CaCu}_3\text{Ti}_4\text{O}_{12}$ films [20], and increasing the O_2 flow rate from 10% to 50% significantly increased the transmittance from 13% to 68% of copper oxide films [21]. NiO films, in particular, exhibit interesting structural properties under different RF sputter conditions and provide multifunctional properties. Prajesh et al. [25] studied the properties of NiO films prepared using the reactive sputtering technique by controlling the Ar: O_2 gas ratios and found that the best structural properties were obtained with a 70:30 Ar: O_2 . The crystallographic evaluation confirmed the existence of a face-centered cubic phase of NiO and showed a granular structure of the film. Similarly, Iwata et al. [26] produced NiO films using the reactive sputtering method under various O_2 gas flow rates, with a rate of 0.9–1.3 sccm, for use as a resistive switching material. The resistivity of the NiO films was controlled through the preparation method. On the other hand, Jamal et al. [16] studied the electrical resistance and optical band gap of NiO films on soda-lime glass that were prepared using RF magnetron sputtering, varying the substrate temperature from room temperature to 400 °C. The results showed that the NiO films had a preferential orientation of the (200) plane when deposited at 100 °C. The electrical resistance of the films was between 2150 $\Omega\text{-cm}$ to 72 $\Omega\text{-cm}$, depending on the deposition temperature, and the optical band gaps decreased from 3.8 eV to 3.2 eV due to the increased substrate temperature. Kim et al. [27] investigated hetero-junction solar cells using a NiO anode buffer layer between the photo-active and indium layers. The Tin oxide anode layer and NiO anode buffer layer were deposited using the RF magnetron sputtering method, which confirmed the p-type characteristic of the NiO film with a resistivity of 0.35 $\Omega\text{-cm}$. Turgut et al. [28] also produced NiO films under different O_2 pressures, which resulted in the formation of nano pyramids or spherical NiO films depending on the low or high O_2 partial pressure, respectively. The Hall measurements confirmed the p-type conductivity with carrier concentrations of 10^{13} holes/ cm^3 . Dhull et al. [29] showed that sputtered NiO films under O_2 gas pressure resulted in a nano-structured NiO film with increased surface roughness (5.09 nm). The results of the electrochemical and electrical properties showed an increased charge transfer and conductivity, which decreased from 6.72×10^{-6} S/cm to 3.97×10^{-6} S/cm with increasing deposition pressure from 20 mT to 40 mT.

This study aims to investigate the effects of Ar gas pressure and film thickness on the structural, optical, magnetic, and conductive properties of NiO films. To compare experimental results, density functional theory (DFT) calculations were performed to determine the optical band gap and lattice parameters as a function of film thickness and Ar gas pressure. Previous studies have examined some of these properties individually, but, as far as we know, there is no study in the literature that includes all these physical properties of NiO films. Thus, this research investigates how the deposition process parameters affect the properties of NiO films by performing both experimental and theoretical studies to provide a more holistic understanding of physical properties of NiO. The findings of this study can provide useful insights for optimizing the deposition process and enhancing the properties of NiO films for various applications.

2. Experimental methods

2.1. NiO film deposition

In this study, NiO films were deposited on a glass substrate using a NiO target (purchased from Maideli) with a purity of 99.999%, thickness of 0.635 cm, and diameter of 5.08 cm in NANOVAK NVT5-400-2TH2SP RF magnetron sputtering system. The glass substrates were cleaned in acetone for 8–10 min and dried in air. The substrate, with a size of 2.6 cm \times 7.6 cm, was used without pre-heating and rotated at 10 rpm to

ensure film thickness uniformity during deposition. Two groups of samples were investigated: the first one had a constant thickness of \sim 30 nm under different Ar gas pressures of 2, 5, 8, 11, and 23 mTorr and the second had different thicknesses of 30, 80, 124, and 246 nm at a constant pressure of 11 mTorr. For NiO film deposition, the RF sputter technique was used with a power of 118 W and a deposition rate of 0.3 Å/s, while the base pressure was \sim 30 mTorr during deposition. The distance between the substrate and the target was 6.2 cm, and the quartz crystal thickness monitor was placed close to the sample holder.

2.2. NiO characterization

The structural analysis of NiO films was performed using the PANalytical EMPYREAN x-ray diffraction (XRD) system with Cu-K α radiation (40 kV, 30 mA). The crystal parameters of the NiO films were determined through Rietveld refinement analysis using the FullProf software suite. The film thickness and surface topology were measured using the TESCAN Mira3 scanning electron microscopy (SEM) and Park NX10 atomic force microscopy (AFM), respectively. The optical properties of the NiO films were characterized using a double-beam UV–VIS–NIR spectrophotometer (Cary 5000). The electrical properties were studied using the Nanomagnetism HEMS Hall Effect Measurement System, and magnetic measurements were performed using a physical property measurement system with a vibrating sample magnetometer head, as a function of applied field (\pm 3 T) at room temperature.

2.3. DFT calculation

In this study, the elastic and electronic properties of a NiO film were investigated using DFT calculations in the QUANTUM Espresso 6.5 program package [30,31]. A cutoff energy of 140 R γ for the valence electron states and 1904 eV for the charge density in the plane-wave basis set were employed. The local spin density approximation (LSDA) in the Perdew-Wang (PW) function was applied to the antiferromagnetic order in NiO to determine the exchange-correlation energy [32]. The Troullier-Martins norm [33] was used to preserve pseudopotentials for core-electron interactions. The calculations for nickel atoms were performed using Hubbard-corrected DFT energy functions (LSDA + U). The LSDA + U approach and Hubbard model were utilized to account the lack of a DFT-based correlation-exchange function [34–36]. The strong correlation between the 3 d electrons of Ni and on-site Coulomb interaction was taken into account by setting $U = 7.6$ eV.

Considering that the local density approximation may not always accurately reproduce electronic characteristics, especially the band gap, we used the generalized gradient approximation (GGA) with the Perdew-Burke-Ernzerhof (GGA-PBE) functional [37] for the exchange-correlation terms. We employed a Vanderbilt ultrasoft pseudopotential for nickel [38] and PAW-pseudopotential for oxygen [39–41]. Integration of the Brillouin zone was performed using the Monkhorst-Pack k-point sampling scheme [42] with a mesh grid size of $12 \times 12 \times 1$, which was later increased to $24 \times 24 \times 1$ for non-self-consistent field calculations. To eliminate non-physical interactions, we calculated the electronic density of states (DOS) using the Böchl tetrahedron method [43]. We set the interlayer vacuum intervals of all structures to 20 Å.

The NiO films were studied with varying thicknesses using periodic boundary conditions in the XY-plane. The atomic equilibrium positions were obtained by calculating forces and stress to minimize the unit cell. Ionic relaxations between the layers were considered to be 10^{-8} eV with a convergence criterion of self-consistent calculations. The forces acting on the atoms were optimized until they were smaller than 10^{-4} hartree/bohr, which was used to determine the atomic and supercell positions in the structure. We monitored these calculations to ensure that the stress value dropped below 0.01 kbar.

3. Results and discussion

3.1. Structural characterization of NiO films

The crystal structure, lattice parameters, volume and $d_{(111)}$ -spacing of NiO films on a glass substrate were determined using XRD patterns and Rietveld refinement analyses. Fig. 1(a and b) show an example of the Rietveld refinement analyses for 30 nm and 246 nm NiO films, respectively, where black circles represent experimental data, red lines represent simulated fit, blue lines represent difference, and green bars indicate the Bragg positions of the observed peaks. The inset of Fig. 1(a and b) show the atomic structure of the NiO film obtained from the refinement analysis, depicting Ni (red) and O (grey) atoms equally occupying in the structure and a schematic representation of NiO film on glass substrate. Table 1 summarizes the results of the Rietveld refinement analyses of NiO films on a glass substrate, including crystal structure, lattice parameters, volume, and $d_{(111)}$ -spacing.

Fig. 1(c and d) summarize the NiO film deposition at different Ar pressures of 2, 5, 8, 11, and 23 mTorr and at different thicknesses of 30, 80, 124, and 246 nm under constant pressure of 11 mTorr. The crystallinity of 30 nm NiO films was low for samples deposited at low pressures, but increasing the deposition pressure improved the crystallinity and the intensity of the (111) and (200) peaks [44]. A similar behavior was observed for Ni film formation under O_2/Ar gas pressure

Table 1

The summary of Rietveld refinement analyses of the NiO films: crystal structure, lattice parameters, volume, and $d_{(111)}$ -space.

Thickness	Pressure	Crystal Structure	Lattice Parameter $a = b = c$ (Å)	Volume (Å ³)	$d_{(111)}$ -space (Å)
30 nm	2 mTorr	fcc- $fm\bar{3}$	4.0559	66.7228	2.3208
	5 mTorr	m	4.1216	70.0152	2.3794
	8 mTorr		4.1913	73.6301	2.4199
	11 mTorr		4.2527	76.9120	2.4553
	23 mTorr		4.2712	77.9213	2.4582
80 nm	11 mTorr	fcc- $fm\bar{3}$	4.2439	76.4344	2.4500
124 nm	11 mTorr	m	4.2407	76.2636	2.4484
246 nm			4.2389	76.1582	2.4473

[15] as well as different type of films [19,45,46]. All samples displayed a face-centered cubic (fcc) structure with a space group of $fm\bar{3}m$ which is a typical structure for NiO films independent from the RF power, gas pressure and the film thickness [47,48]. For pressure-controlled samples, the lattice parameters and the $d_{(111)}$ -spacing increased from 4.0559 Å to 4.2712 Å and from 2.3208 Å to 2.4582 Å, respectively, due to the increased Ar pressure during NiO film deposition. These lattice parameters are close to 4.16 Å for spin-coated NiO films and 4.19 Å for

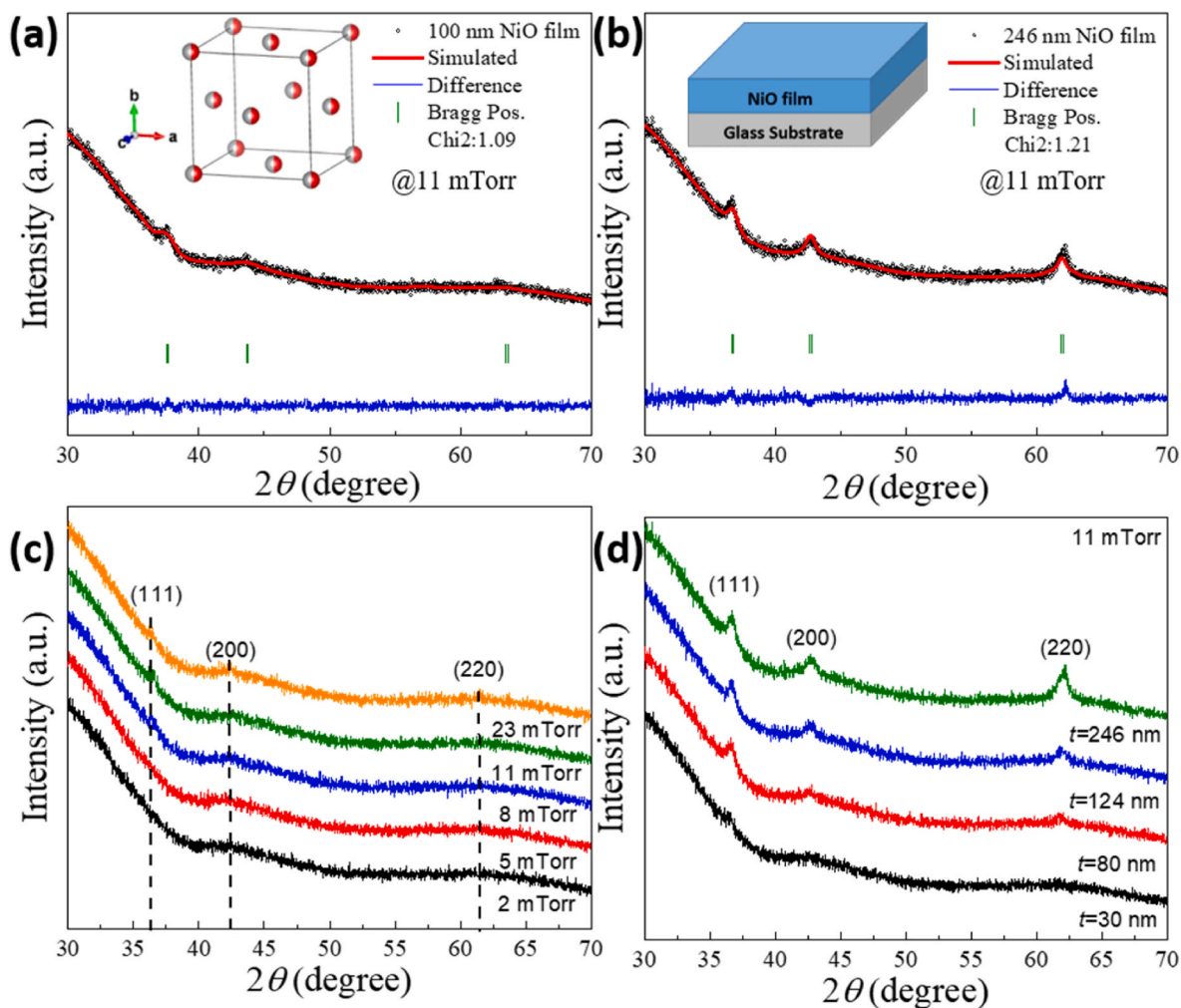


Fig. 1. The XRD profiles of the NiO films. (a and b) Rietveld refinement of 30 nm and 246 nm NiO films with inset atomic structure and a schematic representation of NiO film on glass substrate, experimental data (black circles), calculated patterns (red line), difference (blue line), and Bragg positions (green bar) with Miller indices. (c) NiO films prepared under different pressures (2, 5, 8, 11, and 23 mTorr) and (d) different thicknesses (~30, 80, 124, and 246 nm) at constant pressure of 11 mTorr.

NiO films annealed at 500 °C [49,50], as the film growth is highly dependent on the production process and the type of substrate. It can be concluded that the film growth under Ar gas pressures increases the lattice parameters and atomic distance in the structure.

Moreover, by increasing the Ar gas pressure from 2 to 23 mTorr, the crystallinity improved, and the (111) peak appeared on the XRD profile (see Fig. 1(c)). Increasing the film thickness from 30 nm to 246 nm resulted in an increase in the peaks intensities of (111), (200), and (220) planes. The average crystallite size, D , of NiO films, produced at a constant Ar gas pressure of 11 mTorr, was obtained from Debye–Scherrer equation [14].

$$D = \frac{0.9\lambda}{\beta \cos \theta}$$

Here, λ is the wavelength of Cu-K α radiation (1.54178 Å), β is the Full width at half maximum of the peak and θ is the Bragg angle. The crystallite size of 30, 80, 124, and 246 nm NiO films were found to be 6, 7, 9, and 9 nm, respectively. However, the lattice parameters and $d_{(111)}$ space decreased from 4.2527 Å to 4.2389 Å and from 2.4553 Å to 2.4473 Å, respectively, as the NiO film thickness increased from 30 nm to 246 nm. In conclusion, it can be stated that increasing both the Ar pressure and the film thickness improved the crystallinity of NiO films on the glass substrate.

In this study, the thickness of NiO films was determined using SEM analysis at 10 kV with a 100,000 \times magnification. The cross-sections of NiO films prepared at 11 mTorr Ar gas pressure are shown in Fig. 2(a–d). The average thicknesses were found to be 30.7 nm, 80.2 nm, 124.3 nm, and 246.2 nm, respectively. The SEM images revealed uniform, long-range film formations on the glass substrate. The growth of NiO films using RF magnetron sputtering resulted in thinner films compared to other methods [3,48,49]. The surface topography of the film was

analyzed using tapping mode AFM at a frequency of 326 Hz, a scan rate of 1 Hz, and a scan area of $2.5 \times 2.5 \mu\text{m}^2$. Fig. 3(a) shows almost spherical NiO island formation on the surface with uniform and homogeneous distribution, which is consistent with previous findings in the literature [3,49]. Furthermore, we investigated the average island size via AFM image shown in Fig. 3(a). The average island size was calculated using a lognormal fit with a narrow size distribution between 30 nm and 80 nm, resulting in an average size of 54.28 ± 0.33 nm for NiO islands. This allows for the formation of a uniform and homogeneous film growth.

3.2. Optical properties of NiO films

We first characterized the optical properties of NiO films on a glass substrate by measuring their transmittance and energy band gap values. Glass substrate were chosen due to their transparency, stability, flatness, and availability making them an excellent choice for thin film growth in optical applications [51,52]. Fig. 4(a) displays the optical transmittance spectra of the NiO films as a function of wavelength, for films with a thickness of 30 nm and different Ar pressures. The transmittance percentages of the NiO films on glass increase with increasing Ar gas pressure. As shown in Fig. 4(a), the absorption edge becomes steeper with increasing Ar pressure [52], indicating an improvement in the structural homogeneity and crystallinity of the films, which is confirmed by the XRD and Rietveld refinement analyses. Additionally, we determined the energy band gaps of the NiO films as a function of Ar gas pressure using the $(\alpha E)^2$ vs. E plot as seen in Fig. 4(b). The band gaps were derived using the relations established by Barden et al. [53];

$$\alpha h\nu = B(h\nu - E_g)^m \quad (1)$$

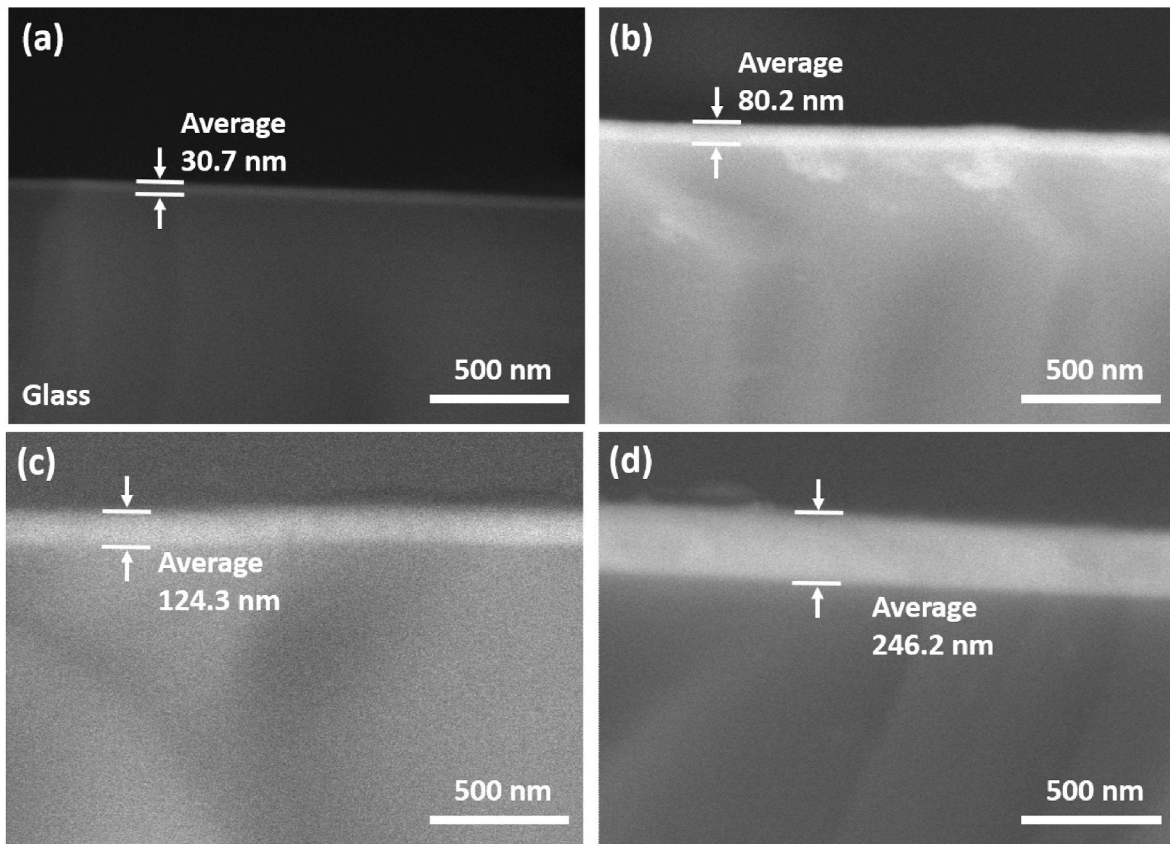


Fig. 2. (a–d) The cross-sections SEM images of as-prepared NiO films with an average thickness of 30.68 nm, 80.22 nm, 124.3 nm, and 246.22 nm, respectively. (Image recorded at 10 kV with 100000 \times magnification).

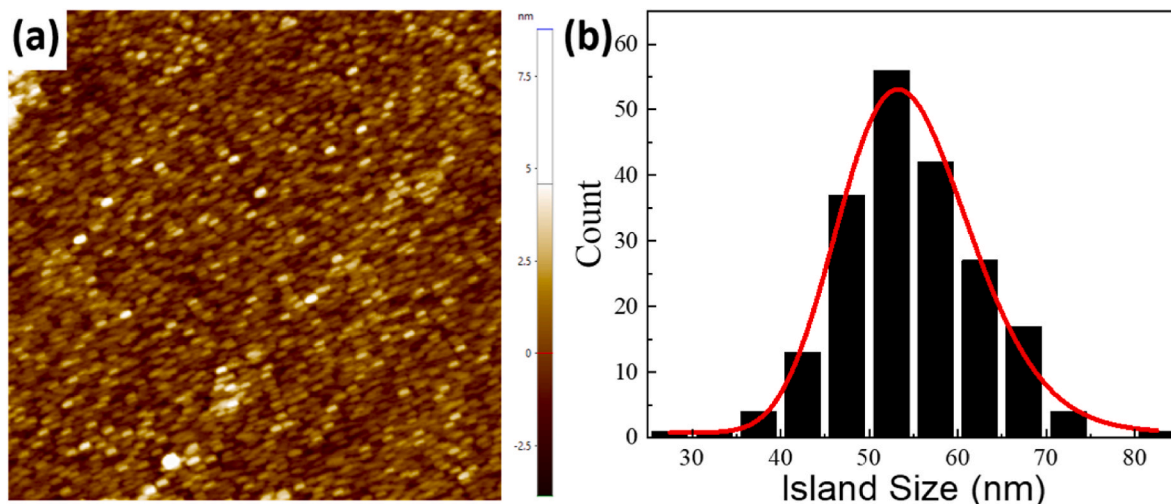


Fig. 3. (a) AFM image reveal the surface topography of 246 nm NiO film on glass substrate with color scale. (b) The average island size of NiO film surface with lognormal fit which is 54.28 ± 0.33 nm (Image recorded with tapping mode, frequency of 326 Hz, scan rate of 1 Hz, and scan area of $2.5 \times 2.5 \mu\text{m}^2$).

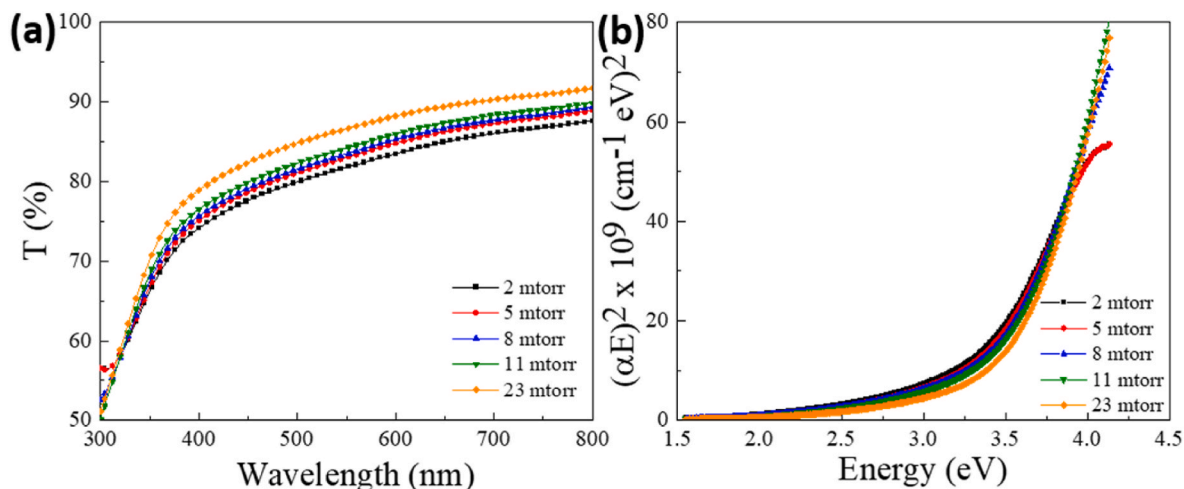


Fig. 4. (a) Variation of transmittance according to wavelength of 30 nm thick NiO films produced on glass at different argon pressures. (b) Variation of $(\alpha E)^2$ with respect to energy to find the direct energy band gap of 30 nm thick NiO films produced on glass at different argon pressures. Change of transmittance according to wavelength of NiO films produced on glass of different thicknesses at 11 mTorr pressure.

$$\alpha E = B(E - E_g)^m \tag{2}$$

Here α , B and E_g represent the absorption coefficient, an independent energy constant, and the energy band gap, respectively. The degree of Equation (2) is represented by m , which determines the material’s optical transition type. The m value can take on the values $1/2$, $3/2$, 2 , or 3 , indicating direct allowed, direct forbidden, indirect allowed, and indirect forbidden transitions, respectively. By analyzing the steadily increasing region in Fig. 4(b), we calculated the energy band gap of the film by finding the intersections from a linear fit. The direct energy band gaps of all films grown at different pressures were calculated and summarized in Table 2. As seen in Table 2, the E_g value increases from 3.26 eV to 3.55 eV as the pressure increases from 2 mTorr to 23 mTorr. These optical band gaps of bulk NiO fall in the range of 3.2–4.0 eV [7,48]. Thus, Ar gas allows us to control the band gap value during the production process for which similar results were also reported in Table 3 for NiO films [52,54]. The change in the energy band gap values is attributed to the effect of the carrier concentration in the film. In other words, the p state of O (valence bands) and the d state of Ni (conduction band) play a crucial role in the charge-transfer transition in the bulk [55]. However, the observed band gap shift towards lower values in the

Table 2

Band gap energy and Hall Effect measurement results of NiO film on glass substrate as a function of Ar gas pressure and the film thickness.

Pressure (mTorr)	E_g (eV)	Sheet Carrier $\times 10^{10}$ ($1/\text{cm}^2$)	Bulk Carrier $\times 10^{15}$ ($1/\text{cm}^3$)	Type
2	3.26	0.21	8.46	p
5	3.31	2.12	6.83	
8	3.42	4.32	13.9	
11	3.48	5.09	16.4	
23	3.55	11.2	36.0	
Thickness (nm)	E_g (eV)	Sheet Carrier $\times 10^{10}$ ($1/\text{cm}^2$)	Bulk Carrier $\times 10^{15}$ ($1/\text{cm}^3$)	Type
30	3.48	5.09	16.4	p
80	3.61	1.16	1.45	
124	3.65	1.07	0.86	
246	3.65	1.18	0.48	

low Ar gas presence agrees with the sputtered NiO film under $\text{O}_2/\text{Ar} + \text{O}_2$ flow rate [48].

We also conducted similar experiments for NiO films with

Table 3

Summary of the recent studies on NiO thin film growth conditions, band gap (E_g) and semiconductor type.

Film Growth Conditions	E_g (eV)	Type	Refs.
Different Ar gas pressures-thickness of 30, 80, 124, and 246 nm	3.26–3.65	p-type	In this study
As deposited-Annealed at 100, 200, 300, and 400 °C	3.67–3.69	p-type	[63]
RF sputtering power of 80, 100, 120, 140, and 160 W	3.44–3.70	p-type	[62]
RF sputtering power of 90 W–200 nm	3.52–3.56	–	[56]
RF sputtering power of 170, 210, 230, and 250 W-thickness of 150, 200, 250, 300, and 350 nm	3.43–3.45	–	[48]
RF sputtering power of 100, 150, and 200 W	3.12–3.93	p-type	[47]
RF sputtering power of 150 and 200 W-as prepared and annealed at 300 °C	3.40–3.71	p-type	[54]
Different O_2 fluxes	3.53–3.65	p-type	[60]
As deposited-Annealed at 300, 400, and 500 °C	3.18–3.56	–	[51]
RF sputtering power of 50–400 W-different O_2 /Ar pressures-thickness 200 nm	3.18–3.30	p-type	[52]

thicknesses of 30, 80, 124, and 246 nm (refer to Fig. 5(a)). As anticipated, with increasing film thickness, the transmittance decreases due to the thickness effect. As the thickness increases, the interference fringes become more pronounced leading to a decrease in transmittance due to free carrier absorption caused by a rise in carrier density in thicker films [56]. Additionally, we observed that the absorption edge shifts to a longer wavelength as the thickness increases. We calculated the energy band gap values from the linear part of $(\alpha E)^n$ vs. $h\nu$ curves in Fig. 5(b) for films of different thicknesses and summarized in Table 2. These results demonstrate a clear relationship between the energy band gap and film thickness. As seen from Table 2, the band gap increases to higher energies as the thickness increases. This suggests that thicker films have less strain and a higher energy band gap compared to thinner films (see Table 3).

3.3. Hall measurements

The electrical properties of NiO films were determined using Hall Effect measurements performed at RT using the Van der Pauw method. Table 2 presents the sheet carrier, bulk carrier, and Hall coefficient values that were measured for both pressure-dependent and thickness-dependent samples. All NiO films exhibited p-type semiconductor characteristics, consistent with previous findings [44,57]. As the pressure increased from 2 to 23 mTorr, the sheet carrier increased from 0.21

to 11.2×10^{10} ($1/cm^2$), while the film thickness increased, the sheet carrier decreased from 5.09 to 1.18×10^{10} ($1/cm^2$). The bulk carrier exhibited similar behavior to the sheet carrier, with the maximum carrier being 36×10^{15} ($1/cm^3$), which is within the expected range for applications [49]. The change in bulk carrier concentration was dependent on both the surface chemical reactions during the experiment and the structural changes of the films. Increasing the sputtering pressure resulted in oxygen vacancies and thus lattice defects in the film, leading to an increase in carrier concentration. Furthermore, the decrease in carrier concentrations with increasing film thickness might indicate an increase in the crystallinity of NiO films.

3.4. Magnetic properties of NiO films

The magnetic properties of the NiO films were studied by measuring the magnetic hysteresis (M - H) curve at RT by sweeping the applied magnetic field between ± 3 T. Fig. 6 shows M - H curves for the NiO films with thicknesses of 30 (black) and 246 nm (red) grown on the glass substrate. The moment values were normalized by the volume of the

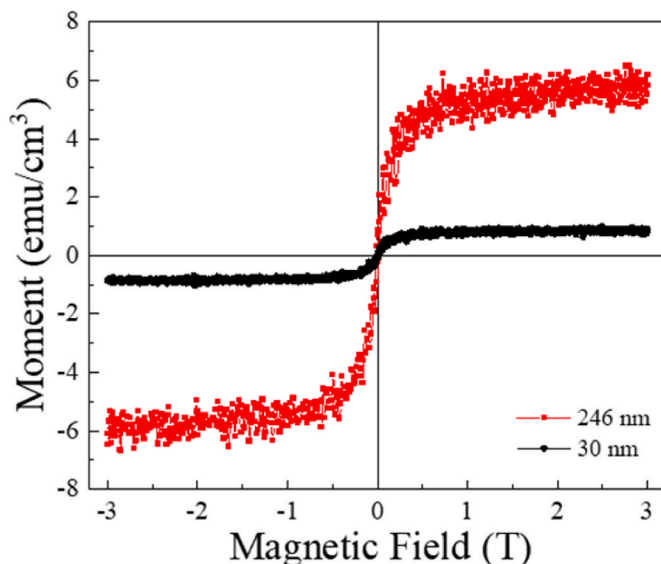


Fig. 6. M vs. H curves for 30 (black) and 246 nm (red) NiO films on glass substrate.

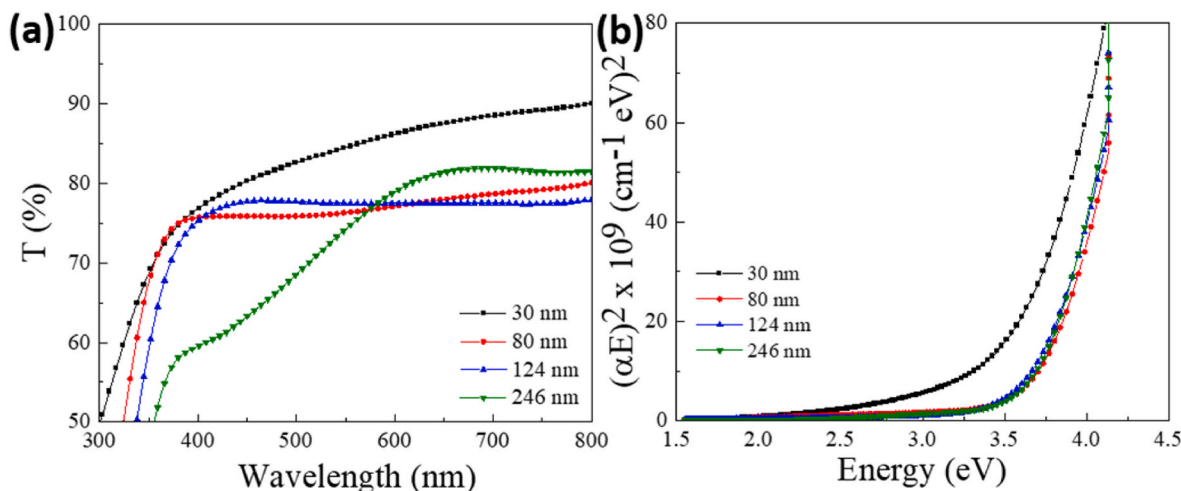


Fig. 5. (a) Variation of transmittance according to wavelength of 11 mTorr films and (b) $(\alpha E)^2$ with respect to energy to find the direct energy band gap of NiO films on glass at different thicknesses.

measured samples. Both samples exhibited a soft magnetic characteristic, with a low coercive field (H_c) and remanent magnetization (M_r) at RT. The saturation magnetization (M_s) of the NiO films for the 30 nm and 246 nm films were found to be 0.84 emu/cm^3 and 5.82 emu/cm^3 , respectively. As shown in Fig. 6, increasing the thickness increased the magnetization in the structure almost 7 times, which is quite comparable to the film thickness, indicating the dependence of M_s on the film thickness. The increase in M_s can be explained by the decomposition of NiO into Ni and/or due to defects such as oxygen vacancies [58]. As the interference fringes were observed in the thicker film (246 nm) in the optical transmittance measurement, the free carriers could be enhanced by the film thickness due to occurrence of defects. The effective magnetic moment, μ_{eff} , values for the films with 30 and 246 nm thickness were found to be $0.011 \mu_B$ and $0.078 \mu_B$. Similarly H_c increased from 81.5 Oe to 178.5 Oe when the thickness increased from 30 nm to 246 nm.

3.5. DFT calculation of NiO film

We investigated the properties of NiO films with varying thicknesses, from one to five layers, and compared them to those of a bulk NiO sample, as depicted in Fig. 7. Prior to analysis, we performed geometry optimization on the NiO films to ensure that no transformations or breaking of interlayer Ni–O bonds had occurred. However, the interlayer bonds in multilayer NiO films were found to be different due to edge effects. For example, in a five-layer NiO film, the bond lengths between the layers were 2.118 and 2.141 Å, while the bond length in a bulk NiO sample was 2.113 Å, which is similar to the average bond length of $2.10 \pm 0.02 \text{ Å}$ observed in previous the experimental work on as-deposited NiO films [59]. The unit cells of the simple square structures were consisted of two (Ni_2O_2), four (Ni_4O_4), six (Ni_6O_6), eight (Ni_8O_8), and ten ($\text{Ni}_{10}\text{O}_{10}$) nickel and oxygen atoms for the one-, two-, three-, four-, and five-layer films, respectively. The optimized lattice constant was found to be 4.00 Å for the one-layer film, 4.10 Å for the two-layer film, 4.06 Å for the three-layer film, 4.13 Å for the four-layer film, and 4.17 Å for the five-layer film. The lattice constant for the simple cubic lattice of the bulk NiO sample was 4.22 Å. These findings also similar with our experimental results and literature [15,44,48,60].

We further investigated the electronic properties of NiO films by determining their DOS, which provides fundamental electronic properties such as the band gap and characteristic peaks. Fig. 8(a–d) show the DOS curves vs. $E-E_F$ for one, two, and five layers, as well as the bulk NiO, with the Fermi level set to zero energy. The DOS nature indicates that the NiO films, as well as the bulk NiO sample, exhibit semiconducting properties, with DOS equal to zero at the Fermi level, a gap, and Van Hove singularities, which are characteristic of two-dimensional materials. The estimated band gaps at the LSDA + U level of theory are 0.66, 1.24, 0.70, 1.14, 1.44, and 2.74 eV for one, two, three, four, five, and infinite layers, respectively. The energy gap increases nonlinearly with an increase in the number of NiO film layers. To refine this value, we repeated the calculations at the GGA + U level of theory ($U = 7.6 \text{ eV}$)

and found the refined gap value to be 3.2 eV (see Fig. 9). It can be suggested that NiO films a few nanometers thick can have a gap close to the 3.2 eV value.

In addition, the mechanical properties of the NiO monolayer were investigated using small strain values, less than 2%, to ensure that the system remains in the elastic region. The elastic properties of the NiO film can be characterized by its linear response to external in-plane stress. In other words, by estimating the in-plane stiffness, which is the equivalent of the two-dimensional Young's modulus. It can be defined as the second derivative of the total energy (E) with respect to the uniaxial strain (ϵ) divided by the equilibrium area of the unit cell S [61] using given formula,

$$Y_{2D} = \frac{1}{S} \frac{\partial^2 E}{\partial \epsilon^2}$$

At the LSDA + U level of theory, we obtained $Y_{2D} = 443 \text{ J/m}^2$.

The results, structural, optical, electrical, magnetic and DFT calculation, indicate that the properties of NiO films are highly dependent on deposition pressure and NiO film thickness (see Table 3) [48,52]. Low deposition pressure resulted in low crystallinity, while increasing deposition pressure improved the crystallinity and peak intensity of NiO films. The lattice parameters and $d_{(111)}$ -spacing also increased with increasing pressure. Furthermore, the crystallite size increased with film thickness, while the lattice parameters and $d_{(111)}$ -spacing decreased. This suggests that increasing both the Ar pressure and film thickness can improve the crystallinity of NiO films on a glass substrate. The increase in E_g value from 3.26 eV to 3.55 eV with increasing pressure can be explained by the change in electronic structure of NiO films with pressure [3,56]. Furthermore, as film thickness increases, the transmittance decreases due to the thickness effect, and interference fringes become more pronounced. This leads to a decrease in transmittance due to free carrier absorption caused by a rise in carrier density in thicker films.

Hall Effect and magnetic measurements were performed as a function of Ar gas pressure and film thickness. The sheet carrier and bulk carrier both exhibited similar behavior with increasing gas pressure and film thickness, with the sheet carrier increasing and the bulk carrier exhibiting a maximum carrier density within the expected range for applications [60,62]. Similarly, the saturation magnetization, effective magnetic moment, and coercivity all increased with increasing film thickness, indicating that thicker films have higher magnetic properties.

DFT calculations were performed to compare experimental results with the structural, optical and electronic properties of NiO films also investigated with. Herein, we investigated the bond lengths up to five-layer NiO film and were found to be similar to the average bond length observed in previous experimental work on as-deposited NiO films. The lattice constant for the simple cubic lattice of bulk NiO was larger than the optimized lattice constants for NiO films with increasing number of layers. The estimated band gaps at the LSDA + U level of theory were found to increase nonlinearly with an increase in the number of NiO film layers. Refining the calculations at the GGA + U level of theory resulted in a refined gap value of 3.2 eV, suggesting that

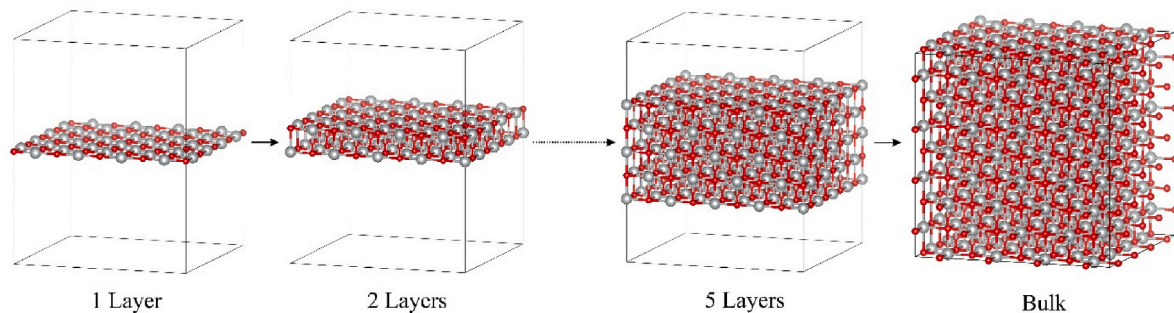


Fig. 7. Atomic structures of the NiO films from one to five layers. Silver and red balls correspond to nickel and oxygen atoms, respectively. The solid black line confines the 4×4 supercell.

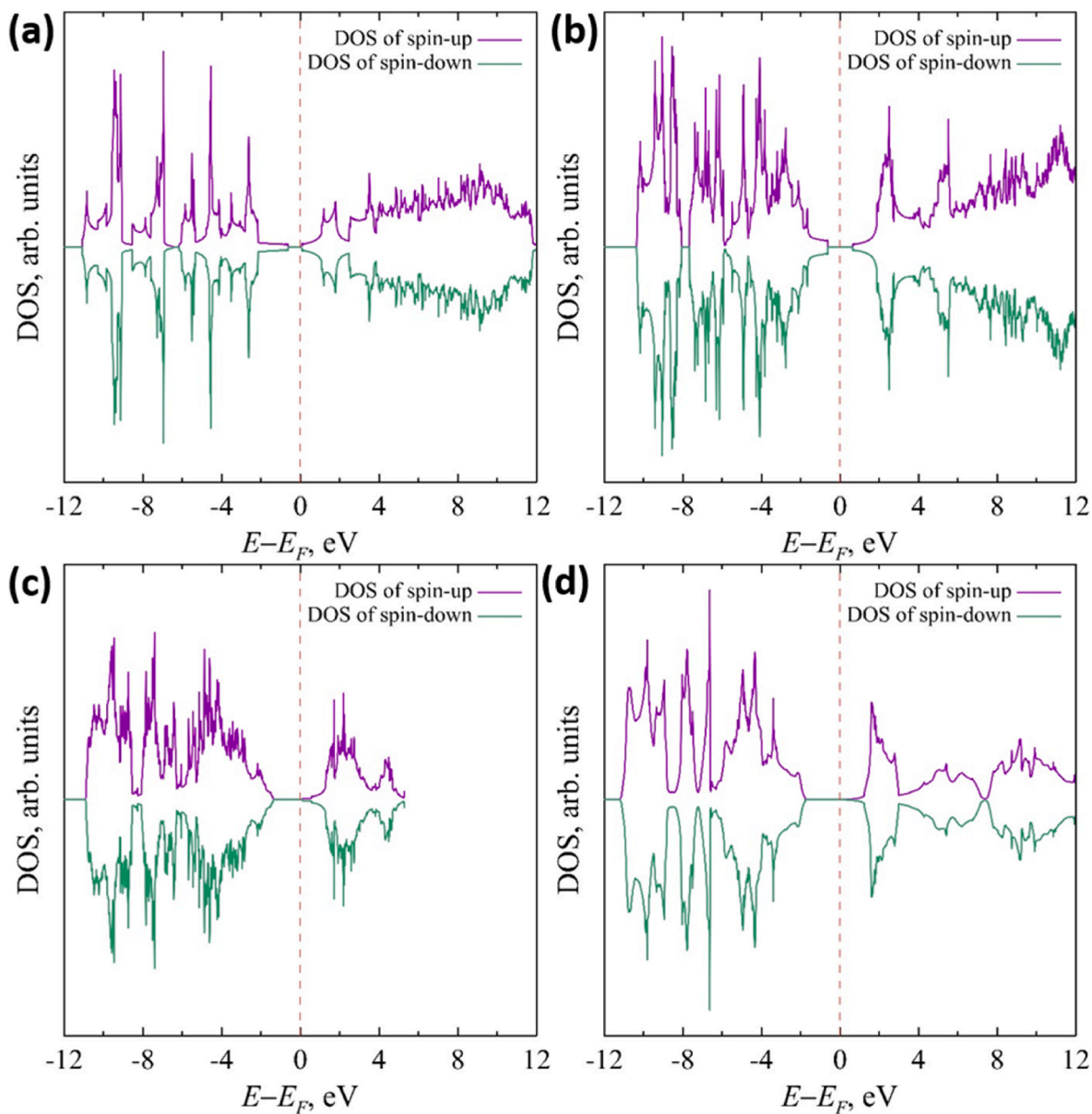


Fig. 8. DOS of the NiO films and bulk sample obtained at the LSDA + U approach: one layer (a), two layers (b), five layers (c), and bulk material (d). The Fermi level is assigned at zero.

NiO films a few nanometers thick can have a gap close to this value. Overall, these results provide insight into the properties of NiO films and their dependence on deposition conditions and film thickness.

4. Conclusion

In summary, NiO films were prepared using the RF magnetron sputtering method with different Argon gas pressures ranging from 2 mTorr to 23 mTorr and thicknesses ranging from 30 nm to 246 nm. The cubic structure of the NiO films was confirmed using XRD and Rietveld refinement analysis, and the maximum lattice parameter and the $d_{(111)}$ -space were found to be 4.2712 Å and 2.4582 Å, respectively, at an Argon gas pressure of 22 mTorr. The thicknesses of the films were confirmed using SEM images, and AFM images revealed a spherical morphology with an average size of 54.28 ± 0.33 nm. The optical band gap values of the films were found to vary from 3.26 to 3.65 eV with increasing pressure, and the p-type characteristic of NiO films was confirmed with an average sheet carrier concentration of 10^{10} cm^{-2} . Soft magnetic

properties were observed, with a maximum H_c of 178.5 Oe and M_s of 5.82 emu/cm^3 for 246 nm NiO film. The electronic properties of NiO films were also investigated using DFT calculations, which optimized the structures of one to five layers of NiO film and bulk NiO formations. The energy gap was found to be 3.2 eV similar to experimental results.

Credit author statement

Hicret Hopoğlu: Data curation; Writing- Original draft preparation. **Dogan Kaya:** Conceptualization; Data curation; Formal analysis; Investigation; Methodology; Validation; Roles/Writing - original draft; Writing - review & editing. **Mikhail M. Maslov:** Data curation; Writing- Original draft preparation. **Savas Kaya:** Data curation; Writing- Original draft preparation. **İlkay Demir:** Data curation; Writing- Original draft preparation. **İsmail Altuntaş:** Data curation; Writing- Original draft preparation. **Fatih Ungan:** Data curation; Writing- Original draft preparation. **Mustafa Akyol:** Data curation; Roles/Writing - original draft; Writing - review & editing. **Ahmet Ekicibil:** Conceptualization;

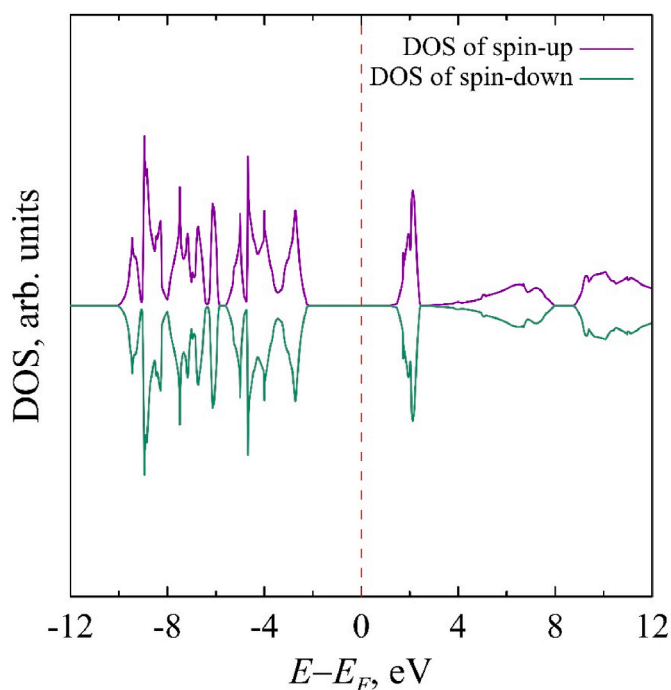


Fig. 9. DOS of the NiO bulk sample obtained at the GGA + U approach. The Fermi level is assigned at zero.

Methodology; Project administration; Roles/Writing - original draft; Writing - review & editing. **Ebru Şenadım Tüzemen:** Conceptualization; Data curation; Formal analysis; Funding acquisition; Methodology; Project administration; Roles/Writing - original draft; Writing - review & editing.

Declaration of competing interest

The authors declare that they have no known competing financial interests or personal relationships that could have appeared to influence the work reported in this paper.

Data availability

Data will be made available on request.

Acknowledgments

This work is supported by the Scientific Research Project Fund of Sivas Cumhuriyet University under the project number F-2021-640. The authors acknowledge the usage of the Nanophotonics Research and Application Center at Sivas Cumhuriyet University (CUNAM), Sivas Cumhuriyet University R&D Center (CUTAM), Cukurova University Department of Physics facilities.

References

- [1] I.-M. Chan, T.-Y. Hsu, F.C. Hong, Enhanced hole injections in organic light-emitting devices by depositing nickel oxide on indium tin oxide anode, *Appl. Phys. Lett.* 81 (2002) 1899–1901.
- [2] M.J. Carey, A.E. Berkowitz, Exchange anisotropy in coupled films of Ni₈₁Fe₁₉ with NiO and Co/Ni_{1-x}O, *Appl. Phys. Lett.* 60 (1992) 3060–3062.
- [3] I. Hotovy, J. Huran, P. Siciliano, S. Capone, L. Spiess, V. Rehacke, The influences of preparation parameters on NiO thin film properties for gas-sensing application, *Sens. Actuators, B* 78 (2001) 126–132.
- [4] S. Itapu, K. Khan, D.G. Georgiev, Effect of UV laser irradiation on the properties of NiO films and ZnO/NiO heterostructures, *MRS Advances* 1 (2016) 293–298.
- [5] H. Sato, T. Minami, S. Takata, T. Yamada, Transparent conducting p-type NiO thin films prepared by magnetron sputtering, *Thin Solid Films* 236 (1993) 27–31.

- [6] B. Subramanian, M. Mohamed Ibrahim, V. Senthilkumar, K.R. Murali, V.S. Vidhya, C. Sanjeeviraja, M. Jayachandran, Optoelectronic and electrochemical properties of nickel oxide (NiO) films deposited by DC reactive magnetron sputtering, *Phys. B Condens. Matter* 403 (2008) 4104–4110.
- [7] V.B. Patil, S.G. Pawar, M. Chougule, P. Godse, R.D. Sakhare, S. Sen, P.J.J.o.S.E.M. Joshi, A. Technology, Effect of annealing on structural, Morphological, Electrical and Optical Studies of Nickel Oxide Thin Films 1 (2011) 35–41.
- [8] H. Hosoi, K. Sueoka, K. Hayakawa, K. Mukasa, Atomic resolved imaging of cleaved NiO(100) surfaces by NC-AFM, *Appl. Surf. Sci.* 157 (2000) 218–221.
- [9] G.A. Niklasson, C.G. Granqvist, Electrochromics for smart windows: thin films of tungsten oxide and nickel oxide, and devices based on these, *J. Mater. Chem.* 17 (2007) 127–156.
- [10] I. Bouessay, A. Rougier, P. Poizat, J. Moscovici, A. Michalowicz, J.M. Tarascon, Electrochromic degradation in nickel oxide thin film: a self-discharge and dissolution phenomenon, *Electrochim. Acta* 50 (2005) 3737–3745.
- [11] J. Nagai, Characterization of evaporated nickel oxide and its application to electrochromic glazing, *Sol. Energy Mater. Sol. Cells* 31 (1993) 291–299.
- [12] Y.-H. You, B.-S. So, J.-H. Hwang, W. Cho, S.S. Lee, T.-M. Chung, C.G. Kim, K.-S. An, Impedance spectroscopy characterization of resistance switching NiO thin films prepared through atomic layer deposition, *Appl. Phys. Lett.* 89 (2006), 222105.
- [13] J.C. Bruyere, B.K. Chakraverty, Switching and negative resistance in thin films of nickel oxide, *Appl. Phys. Lett.* 16 (1970) 40–43.
- [14] M. Ahmadipour, M.J. Abu, M.F. Ab Rahman, M.F. Ain, Z.A. Ahmad, Assessment of crystallite size and strain of CaCu₃Ti₄O₁₂ prepared via conventional solid-state reaction, *Micro & Nano Lett.* 11 (2016) 147–150.
- [15] F. Şenaslın, M. Taşdemir, A. Çelik, Effect of working pressure and post-annealing on structural, optical and electrical properties of p-type NiO thin films produced by RF magnetron sputtering technique, *Appl. Phys. A* 127 (2021) 739.
- [16] M.S. Jamal, S.A. Shahahmadi, P. Chelvanathan, H.F. Alharbi, M.R. Karim, M. Ahmad Dar, M. Luqman, N.H. Alharthi, Y.S. Al-Harathi, M. Aminuzzaman, N. Asim, K. Sopian, S.K. Tiong, N. Amin, M. Akhtaruzzaman, Effects of growth temperature on the photovoltaic properties of RF sputtered undoped NiO thin films, *Results Phys.* 14 (2019), 102360.
- [17] P.V.M. Shameem, L. Mekala, M.S. Kumar, Exchange bias induced by the spin glass-like surface spins in sputter deposited Fe₃O₄ thin films, *IEEE Trans. Magn.* 53 (2017) 1–5.
- [18] A.-C. Sun, F.-T. Yuan, J.-H. Hsu, H.Y. Lee, Evolution of structure and magnetic properties of sputter-deposited CoPt thin films on MgO(111) substrates: formation of the L11 phase, *Scripta Mater.* 61 (2009) 713–716.
- [19] M. Ahmadipour, M. Arjmand, M.F. Ain, Z.A. Ahmad, S.-Y. Pung, Effect of Ar:N₂ flow rate on morphology, optical and electrical properties of CCTO thin films deposited by RF magnetron sputtering, *Ceram. Int.* 45 (2019) 15077–15081.
- [20] M. Ahmadipour, M.F. Ain, Z.A. Ahmad, Effects of annealing temperature on the structural, morphology, optical properties and resistivity of sputtered CCTO thin film, *J. Mater. Sci. Mater. Electron.* 28 (2017) 12458–12466.
- [21] H. El Aakib, N. Rochdi, A. Tchenka, J.-F. Pierson, A. Outzourhit, Copper oxide coatings deposited by reactive radio-frequency sputtering for solar absorber applications, *Mater. Chem. Phys.* 296 (2023), 127196.
- [22] M. Ahmadipour, S.N. Ayub, M.F. Ain, Z.A. Ahmad, Structural, surface morphology and optical properties of sputter-coated CaCu₃Ti₄O₁₂ thin film: influence of RF magnetron sputtering power, *Mater. Sci. Semicond. Process.* 66 (2017) 157–161.
- [23] A.D. Sytchenko, N.S. Kozlova, E.V. Zabelina, P.A. Loginov, E.A. Levashov, P. V. Kiryukhantsev-Korneev, The effect of the Ar/N₂ gas ratio on the structure and properties of Ta-Si-N coatings produced by magnetron sputtering of TaSi₂ target, *Surface. Interfac.* 37 (2023), 102654.
- [24] T. Zhou, L. Pan, Y. Ma, S. Zhu, G. Tan, Q. Man, Origin of high-frequency magnetic loss of Y₃Fe₅O₁₂ single crystal thin films prepared with high-throughput screening by magnetron sputtering, *Vacuum* 207 (2023), 111644.
- [25] R. Prajesh, V. Goyal, M. Nahid, V. Saini, A.K.r. Singh, A.K.r. Sharma, J. Bhargava, A. Agarwal, Nickel Oxide (NiO) Thin Film Optimization by Reactive Sputtering for Highly Sensitive Formaldehyde Sensing, *Sensors and Actuators B, Chemical*, 2020.
- [26] T. Iwata, Y. Nishi, T.J.T.S.F. Kimoto, Grain-boundary structures and their impact on the electrical properties of NiO films deposited by reactive sputtering, *Thin Solid Films* 709 (2020), 138203.
- [27] J. Kim, Y. Ko, K. Park, Effect of RF magnetron sputtered nickel oxide thin films as anode buffer layer in a P 3 HT:PCBM bulk hetero-junction solar cells, *Acta Phys. Pol., A* 133 (2018) 887–891.
- [28] E. Turgut, Ö. Çoban, S. Sarıtaş, S. Tüzemen, M. Yıldırım, E. Gür, Oxygen partial pressure effects on the RF sputtered p-type NiO hydrogen gas sensors, *Appl. Surf. Sci.* 435 (2018) 880–885.
- [29] N. Dhull, G. Kaur, V. Gupta, M. Tomar, Development of nanostructured nickel oxide thin film matrix by rf sputtering technique for the realization of efficient bioelectrode, *Vacuum* 158 (2018) 68–74.
- [30] P. Giannozzi, O. Andreussi, T. Brumme, O. Bunau, M. Buongiorno Nardelli, M. Calandra, R. Car, C. Cavazzoni, D. Ceresoli, M. Cococcioni, N. Colonna, I. Carnimeo, A. Dal Corso, S. de Gironcoli, P. Delugas, R.A. DiStasio, A. Ferretti, A. Floris, G. Fratesi, G. Fugallo, R. Gebauer, U. Gerstmann, F. Giustino, T. Gorni, J. Jia, M. Kawamura, H.Y. Ko, A. Kokalj, E. Küçükbenli, M. Lazzeri, M. Marsili, N. Marzari, F. Mauri, N.L. Nguyen, H.V. Nguyen, A. Otero-de-la-Roza, L. Paulatto, S. Poncè, D. Rocca, R. Sabatini, B. Santra, M. Schlipf, A.P. Seitsonen, A. Smogunov, I. Timrov, T. Thonhauser, P. Umari, N. Vast, X. Wu, S. Baroni, Advanced capabilities for materials modelling with Quantum ESPRESSO, *J. Phys. Condens. Matter* 29 (2017), 465901.
- [31] P. Giannozzi, S. Baroni, N. Bonini, M. Calandra, R. Car, C. Cavazzoni, D. Ceresoli, G.L. Chiarotti, M. Cococcioni, I. Dabo, A. Dal Corso, S. de Gironcoli, S. Fabris, G. Fratesi, R. Gebauer, U. Gerstmann, C. Gougoussis, A. Kokalj, M. Lazzeri,

- L. Martin-Samos, N. Marzari, F. Mauri, R. Mazzarello, S. Paolini, A. Pasquarello, L. Paulatto, C. Sbraccia, S. Scandolo, G. Sclauzero, A.P. Seitsonen, A. Smogunov, P. Umari, R.M. Wentzcovitch, Quantum espresso: a modular and open-source software project for quantum simulations of materials, *J. Phys. Condens. Matter* 21 (2009), 395502.
- [32] J.P. Perdew, Y. Wang, Accurate and simple analytic representation of the electron-gas correlation energy, *Phys. Rev. B* 45 (1992) 13244–13249.
- [33] N. Troullier, J.L. Martins, Efficient pseudopotentials for plane-wave calculations, *Phys. Rev. B* 43 (1991) 1993–2006.
- [34] V.I. Anisimov, I.V. Solovyev, M.A. Korotin, M.T. Czyżyk, G.A. Sawatzky, Density-functional theory and NiO photoemission spectra, *Phys. Rev. B* 48 (1993) 16929–16934.
- [35] V.I. Anisimov, J. Zaanen, O.K. Andersen, Band theory and mott insulators: hubbard U instead of stoner I, *Phys. Rev. B* 44 (1991) 943–954.
- [36] M. Cococcioni, S. de Gironcoli, Linear response approach to the calculation of the effective interaction parameters in the LDA+U method, *Phys. Rev. B* 71 (2005), 035105.
- [37] J.P. Perdew, K. Burke, M. Ernzerhof, Generalized gradient approximation made simple, *Phys. Rev. Lett.* 77 (1996) 3865–3868.
- [38] D. Vanderbilt, Soft self-consistent pseudopotentials in a generalized eigenvalue formalism, *Phys. Rev. B* 41 (1990) 7892–7895.
- [39] P.E. Blöchl, Projector augmented-wave method, *Phys. Rev. B* 50 (1994) 17953–17979.
- [40] G. Kresse, D. Joubert, From ultrasoft pseudopotentials to the projector augmented-wave method, *Phys. Rev. B* 59 (1999) 1758–1775.
- [41] A. Dal Corso, Pseudopotentials periodic table: from H to Pu, *Comput. Mater. Sci.* 95 (2014) 337–350.
- [42] H.J. Monkhorst, J.D. Pack, Special points for Brillouin-zone integrations, *Phys. Rev. B* 13 (1976) 5188–5192.
- [43] P.E. Blöchl, O. Jepsen, O.K. Andersen, Improved tetrahedron method for Brillouin-zone integrations, *Phys. Rev. B* 49 (1994) 16223–16233.
- [44] D. Kaya, H.S. Aydınoglu, E. Şenadım Tüzemen, A. Ekicibil, Investigation of optical, electronic, and magnetic properties of p-type NiO thin film on different substrates, *Thin Solid Films* 732 (2021), 138800.
- [45] M. Ahmadipour, M.F. Ain, S. Goutham, Z.A. Ahmad, Effects of deposition time on properties of CaCu₃Ti₄O₁₂ thin film deposited on ITO substrate by RF magnetron sputtering at ambient temperature, *Ceram. Int.* 44 (2018) 18817–18820.
- [46] D.K. Kim, H.B. Kim, Room temperature deposition of Al-doped ZnO thin films on glass by RF magnetron sputtering under different Ar gas pressure, *J. Alloys Compd.* 509 (2011) 421–425.
- [47] K.S. Usha, R. Sivakumar, C. Sanjeeviraja, Optical Constants and Dispersion Energy Parameters of NiO Thin Films Prepared by Radio Frequency Magnetron Sputtering Technique, vol. 114, 2013, 123501.
- [48] T. Potlog, L. Ghimpu, V. Suman, A. Pantazi, M. Enachescu, Influence of RF sputtering power and thickness on structural and optical properties of NiO thin films, *Mater. Res. Express* 6 (2019), 096440.
- [49] A.A. Ahmed, M.R. Hashim, M. Rashid, Control of the structural, electrical and optical properties of spin coated NiO films by varying precursor molarity, *Thin Solid Films* 690 (2019), 137554.
- [50] A.K. Srivastava, S. Thota, J. Kumar, Preparation, microstructure and optical absorption behaviour of NiO thin films, *J. Nanosci. Nanotechnol.* 8 (2008) 4111–4115.
- [51] G.-J. Chen, C.-M. Lin, Y.-H. Shih, S.-R. Jian, The microstructures and characteristics of NiO films, *Effects of Substrate Temperature* 13 (2022) 1940.
- [52] M.L. Grilli, F. Menchini, T. Dikonimos, P. Nunziante, L. Pilloni, M. Yilmaz, A. Piegari, A. Mittiga, Effect of Growth Parameters on the Properties of RF-Sputtered Highly Conductive and Transparent P-type NiO_x Films, vol. 31, 2016, 055016.
- [53] J. Bardeen, F. Blatt, L.J.W. Hall, New York, in: Photoconductivity Conference, 1956, 195623, 146.
- [54] M. Guzewicz, J. Grochowski, M. Borysiewicz, E. Kaminska, J. Domagala, W. Rzdokiewicz, B. Witkowski, K. Golaszewska, R. Kruszk, M. Ekielski, A. Piotrowska, Electrical and Optical Properties of NiO Films Deposited by Magnetron Sputtering, *XLI, Optica Applicata*, 2011, pp. 431–440.
- [55] G. Madhu, V. Biju, Effect of Ni²⁺ and O²⁻ vacancies on the electrical and optical properties of nanostructured nickel oxide synthesized through a facile chemical route, *Physica E* 60 (2014) 200–205.
- [56] M. Terlemezoglu, O. Surucu, M. Isik, N.M. Gasanly, M. Parlak, Temperature-dependent optical characteristics of sputtered NiO thin films, *Appl. Phys. A* 128 (2021) 50.
- [57] T.-H. Chuang, C.-K. Wen, S.-C. Chen, M.-H. Liao, F. Liu, H.J.C.I. Sun, p-type semi-transparent conductive NiO films with high deposition rate produced by superimposed high power impulse magnetron sputtering, *Ceram. Int.* 46 (2020) 27695–27701.
- [58] P. Ravikumar, B. Kisan, A. Perumal, Thickness dependent ferromagnetism in thermally decomposed NiO thin films, *J. Magn. Magn Mater.* 418 (2016) 86–91.
- [59] Y.R. Denny, K. Lee, C. Park, S.K. Oh, H.J. Kang, D.-S. Yang, S. Seo, Electronic, electrical and optical properties of undoped and Na-doped NiO thin films, *Thin Solid Films* 591 (2015) 255–260.
- [60] H. Cao, G. Hu, X. Hao, L. Wu, D. Zhao, Influence of oxygen flux on properties of nickel oxide films prepared by magnetron sputtering for alternative hole-transporting layer in inverted perovskite solar cells, *J. Mater. Sci. Mater. Electron.* 34 (2023).
- [61] K.P. Katin, K.S. Grishakov, M.A. Gimaldinova, M.M. Maslov, Silicon rebirth: ab initio prediction of metallic sp³-hybridized silicon allotropes, *Comput. Mater. Sci.* 174 (2020), 109480.
- [62] Y. Zhao, H. Wang, F. Yang, Z. Wang, J. Li, Y. Gao, Z. Feng, X. Li, Z.J.M.R. Zhen, Sputtering Power Induced Physical Property Variation of Nickel Oxide Films by Radio Frequency Magnetron Sputtering, 2018, p. 21.
- [63] C. Park, J. Kim, K. Lee, S.K. Oh, H.-j. Kang, N.S.J.A.S. Park, C. Technology, Electronic, optical and electrical properties of nickel oxide thin films grown by RF, Magnetron Sputtering 24 (2015) 72–76.

The power of the Web of Science™ on your mobile device, wherever inspiration strikes.

Dismiss

Learn More

Already have a manuscript?

Use our Manuscript Matcher to find the best relevant journals!

Find a Match

Filters

Clear All


Web of Science Coverage 

Open Access  

Category 

Country / Region 

Language 

Frequency 

Journal Citation Reports 

Refine Your Search Results

PHYSICA B-CONDENSED MATTER

Search

Sort By: Relevancy 

Search Results

Found 115 results (Page 1)

[Share These Results](#)

Exact Match Found

PHYSICA B-CONDENSED MATTER

Publisher: ELSEVIER , RADARWEG 29, AMSTERDAM, Netherlands, 1043 NX

ISSN / eISSN: 0921-4526 / 1873-2135

Web of Science Core Collection: Science Citation Index Expanded

Additional Web of Science Indexes: Current Contents Physical, Chemical & Earth Sciences | Essential Science Indicators

[Share This Journal](#)

[View profile page](#)

* Requires free login.

Other Possible Matches

ADVANCES IN CONDENSED MATTER PHYSICS

Publisher: HINDAWI LTD , ADAM HOUSE, 3RD FLR, 1 FITZROY SQ, LONDON, ENGLAND, W1T 5HF

ISSN / eISSN: 1687-8108 / 1687-8124

Web of Science Core Collection: Science Citation Index Expanded

Additional Web of Science Indexes: Current Contents Physical, Chemical & Earth Sciences | Essential Science Indicators

[Share This Journal](#)

[View profile page](#)

* Requires free login.

ANNUAL REVIEW OF CONDENSED MATTER PHYSICS



Publisher: ANNUAL REVIEWS , 4139 EL CAMINO WAY, PO BOX 10139, PALO ALTO, USA, CA, 94303-0139

ISSN / eISSN: 1947-5454 / 1947-5462

Web of Science Core Collection: Science Citation Index Expanded

Additional Web of Science Indexes: Essential Science Indicators

[Share This Journal](#)

[View profile page](#)

* Requires free login.

COMPUTATIONAL CONDENSED MATTER

Publisher: ELSEVIER , RADARWEG 29, AMSTERDAM, Netherlands, 1043 NX

ISSN / eISSN: 2352-2143

Web of Science Core Collection: Emerging Sources Citation Index

[Share This Journal](#)

[View profile page](#)

* Requires free login.

CONDENSED MATTER

OPEN ACCESS

Publisher: MDPI , ST ALBAN-ANLAGE 66, BASEL, SWITZERLAND, CH-4052

ISSN / eISSN: 2410-3896

Web of Science Core Collection: Emerging Sources Citation Index

[Share This Journal](#)

[View profile page](#)

* Requires free login.

CONDENSED MATTER PHYSICS

OPEN ACCESS

Publisher: INST CONDENSED MATTER PHYSICS NATL ACAD SCIENCES UKRAINE , 1 SVIENTSITSKII STR, LVIV, UKRAINE, 79011

ISSN / eISSN: 1607-324X / 2224-9079

Web of Science Core Collection: Science Citation Index Expanded

Additional Web of Science Indexes: Current Contents Physical, Chemical & Earth Sciences | Essential Science Indicators

[Share This Journal](#)

[View profile page](#)

* Requires free login.

JOURNAL OF CONDENSED MATTER NUCLEAR SCIENCE

Publisher: INT SOC CONDENSED MATTER NUCLEAR SCIENCE , INT SOC CONDENSED MATTER NUCLEAR SCIENCE, KIDDERMINSTER, ENGLAND, 00000

ISSN / eISSN: 2227-3123

Web of Science Core Collection: Emerging Sources Citation Index



[Share This Journal](#)

[View profile page](#)

* Requires free login.

JOURNAL OF PHYSICS-CONDENSED MATTER

Publisher: IOP PUBLISHING LTD , TEMPLE CIRCUS, TEMPLE WAY, BRISTOL, ENGLAND, BS1 6BE

ISSN / eISSN: 0953-8984 / 1361-648X

Web of Science Core Collection: Science Citation Index Expanded

Additional Web of Science Indexes: **Current Contents Electronics & Telecommunications Collection | Current Contents Physical, Chemical & Earth Sciences | Essential Science Indicators**

[Share This Journal](#)

[View profile page](#)

* Requires free login.

PHYSICA C-SUPERCONDUCTIVITY AND ITS APPLICATIONS

Publisher: ELSEVIER , RADARWEG 29, AMSTERDAM, Netherlands, 1043 NX

ISSN / eISSN: 0921-4534 / 1873-2143

Web of Science Core Collection: Science Citation Index Expanded

Additional Web of Science Indexes: **Current Contents Physical, Chemical & Earth Sciences | Essential Science Indicators**

[Share This Journal](#)

[View profile page](#)

* Requires free login.

PHYSICA E-LOW-DIMENSIONAL SYSTEMS & NANOSTRUCTURES

Publisher: ELSEVIER , RADARWEG 29, AMSTERDAM, Netherlands, 1043 NX

ISSN / eISSN: 1386-9477 / 1873-1759

Web of Science Core Collection: Science Citation Index Expanded

Additional Web of Science Indexes: **Current Contents Physical, Chemical & Earth Sciences | Essential Science Indicators**

[Share This Journal](#)

[View profile page](#)

* Requires free login.

Items per page: 10 ▾ 1 – 10 of 115 << < > >>

Editorial Disclaimer: As an independent organization, Clarivate does not become involved in and is not responsible for the editorial management of any journal or the business practices of any publisher. Publishers are accountable for their journal performance and compliance with ethical publishing standards. The views and opinions expressed in any journal are those of the author(s) and do not necessarily reflect the views or opinions of Clarivate. Clarivate remains neutral in relation to territorial disputes, and allows journals, publishers, institutes and authors to specify their address and affiliation details including territory.

Criteria for selection of newly submitted titles and re-evaluation of existing titles in the Web of Science are determined by the Web of Science Editors in



their sole discretion. If a publisher's editorial policy or business practices negatively impact the quality of a journal, or its role in the surrounding literature of the subject, the Web of Science Editors may decline to include the journal in any Clarivate product or service. The Web of Science Editors, in their sole discretion, may remove titles from coverage at any point if the titles fail to maintain our standard of quality, do not comply with ethical standards, or otherwise do not meet the criteria determined by the Web of Science Editors. If a journal is deselected or removed from coverage, the journal will cease to be indexed in the Web of Science from a date determined by the Web of Science Editors in their sole discretion – articles published after that date will not be indexed. The Web of Science Editors' decision on all matters relating to journal coverage will be final.

Clarivate.™ Accelerating innovation.

[© 2023 Clarivate](#)

[Legal center](#)

[Privacy notice](#)

[Cookie policy](#)

[Tanımlama Bilgisi Ayarları](#)

[Copyright notice](#)

[Help](#)

